ChemComm

COMMUNICATION

View Article Online
View Journal | View Issue

Cite this: *Chem. Commun.*, 2019, **55**, 4805

Received 4th March 2019,
Accepted 25th March 2019

DOI: 10.1039/c9cc01758e

rsc.li/chemcomm

In situ formation of electronically coupled superlattices of $Cu_{1.1}S$ nanodiscs at the liquid/air interface†

Sonam Maiti,[ab] Santanu Maiti,[a]* Andre Maier,[b] Rupak Banerjee,[c] Chen Shen,[d] Bridget M. Murphy,[ef] Marcus Scheele[bg] and Frank Schreiber[ag]

We report on the *in situ* monitoring of the formation of conductive superlattices of $Cu_{1.1}S$ nanodiscs *via* cross-linking with semiconducting cobalt 4,4′,4″,4‴-tetraaminophthalocyanine (CoTAPc) molecules at the liquid/air interface by real-time grazing incidence small angle X-ray scattering (GISAXS). We determine the structure, symmetry and lattice parameters of the superlattices, formed during solvent evaporation and ligand exchange on the self-assembled nanodiscs. $Cu_{1.1}S$ nanodiscs self-assemble into a two-dimensional hexagonal superlattice with a minor in-plane contraction (~0.2 nm) in the lattice parameter. A continuous contraction of the superlattice has been observed during ligand exchange, preserving the initial hexagonal symmetry. We estimate a resultant decrement of about 5% in the in-plane lattice parameters. The contraction is attributed to the continuous replacement of the native oleylamine surface ligands with rigid CoTAPc. The successful cross-linking of the nanodiscs is manifested in terms of the high electrical conductivity observed in the superlattices. This finding provides a convenient platform to understand the correlation between the structure and transport of the coupled superstructures of organic and inorganic nanocrystals of anisotropic shape.

Self-assembly of nanocrystals (NCs) into ordered structures has garnered increased attention due to their astonishing properties which are valuable for fundamental studies and technological devices.[1–12] Most of the as-prepared NCs are usually spherical in shape and produce essentially non-conductive superlattices as they feature insulating surface ligands. Relatively little research has been carried out to improve the physical properties of the superlattices by tuning the shape of the NCs, passivating the surfaces of the NCs and cross-linking with organic semiconductor (OSC) molecules.[13–16] Superstructures of copper sulfide nanomaterials have demonstrated generous use due to their rich transport and plasmonic properties.[17–21] The controlled preparation of two dimensional ordered and conductive assemblies of NCs with anisotropic shape is one of the challenges in nano-fabrication as the overall properties of the assemblies depend on their shape and orientation.[22–24] Recently, the physical properties of nanoparticle superstructures coupled electronically with OSC molecules have been investigated by *ex situ* measurements.[25,26] In such a typical superlattice, the OSC molecules bind at certain facets of the NCs with their reactive groups as they have a strong preference to couple between NCs. This might promote high charge carrier transport across the superstructure through resonant energy levels. In spite of the growing importance in the field of fabrication of conductive superstructures by tuning the shape of the NCs, the exact formation mechanism revealing the process is still poorly understood. Here, we use this approach to fabricate a superlattice with interesting transport properties by (a) tuning the shape of the NCs, (b) passivating the NCs' surfaces, and (c) cross-linking with OSC molecules and following the structure formation in real time.

We choose *in situ* grazing incidence small angle X-ray scattering (GISAXS),[11,27,28] which is particularly relevant to elucidating the structure formation in real-time during the involved chemical processes, starting from the self-assembly to ligand exchange. In this context, GISAXS is crucial to determine the *in situ* structural changes in the thin film at the liquid/air interface. We report the *in situ* formation of a conductive hexagonal superlattice of $Cu_{1.1}S$ nanodiscs (NDs) by exchanging the native oleylamine (Olm) surface ligand with CoTAPc at the dimethyl sulfoxide (DMSO)/air interface. Initially, the nanodiscs (core diameter 12.7 ± 0.5 nm and thickness 5.8 ± 0.2 nm)

[a] *Institute of Applied Physics, University of Tübingen, Auf der Morgenstelle 10, 72076 Tübingen, Germany. E-mail: santanu.maiti@uni-tuebingen.de*
[b] *Institute of Physical and Theoretical Chemistry, University of Tübingen, Auf der Morgenstelle 18, 72076 Tübingen, Germany*
[c] *Department of Physics, Indian Institute of Technology Gandhinagar, Palaj, Gandhinagar 382355, India*
[d] *Deutsches Elektronen-Synchrotron DESY, Notkestraße 85, D-22607 Hamburg, Germany*
[e] *Institute for Experimental and Applied Physics, Kiel University, D-24098 Kiel, Germany*
[f] *Ruprecht-Haensel Laboratory, Kiel, 24118, Germany*
[g] *Center for Light-Matter Interaction, Sensors & Analytics LISA+, University of Tübingen, Auf der Morgenstelle 15, 72076 Tübingen, Germany*

† Electronic supplementary information (ESI) available. See DOI: 10.1039/c9cc01758e

self-assemble into a two dimensional (2D) hexagonal superlattice after spreading them on the liquid surface with almost unaltered lattice parameters. A continuous contraction of the in-plane lattice parameters occurs during ligand exchange, preserving the 2D hexagonal structure on the liquid surface. The replacement of Olm with CoTAPc ligands in these superlattice films is confirmed by *ex situ* Raman spectroscopy. A dramatic increase in the conductivity by more than 6 orders of magnitude of the ligand exchanged films suggests that the phthalocyanine derivative acts as an electronic linker between the NDs.

Self-assembly of oleylamine-capped nanodiscs at the DMSO/air interface. Self-assembly of Olm-capped $Cu_{1.1}S$ NDs (Fig. S1a, ESI†) has been monitored by dispersing 200 μL, 5 μM NC solution in toluene at the DMSO/air interface in a custom-built Teflon cell with a surface area of 3×4 cm^2. *In situ* GISAXS patterns are collected as a function of waiting time at intervals of 4–6 minutes during the self-assembly process. Fig. 1a and b show the GISAXS patterns for waiting periods of 5 minutes and 240 minutes, whereas others at intermediate times are shown in the ESI† (Fig. S2). The appearance of several scattering peaks along the in-plane direction (q_y) corresponds to the formation of ordered superlattices. Scattering peaks in the in-plane direction are observed at relative q_y-values of $1:\sqrt{3}:2$, which is characteristic of a 2D hexagonal superlattice, and are indexed to the (10), (11) and (20) lattice planes, respectively. During the self-assembly process, all the GISAXS patterns show resemblance among themselves, which illustrates that the superlattices remain in a hexagonal geometry for the whole assembling time period. The scattering peaks in the GISAXS patterns are fitted by the distorted wave Born approximation (DWBA)[27,29–31] method considering a model of a 2D hexagonal superlattice with suitable lattice parameters (a, b, c = Inf., $\alpha = \beta = 90°$, $\gamma = 120°$, $\theta_c = 0.1°$) and *P6mm* space group (S.G.) symmetry oriented with the $[001]_{SL}$-axis perpendicular to the liquid substrate. We found a small contraction in the lattice parameter ($\sim$0.2 nm) during the first $\sim$40 minutes of self-assembly and almost unaltered $a = b = 16.8 \pm 0.1$ nm for the remaining self-assembly period (until 240 minutes) as shown in Fig. 1c. The obtained lattice parameters also imply that the nanodiscs assemble into a 2D hexagonal superlattice with an edge-to-edge configuration. Fig. 1d shows that the in-plane scattering peaks show no shift in the extracted line profiles of the GISAXS patterns, obtained at different time intervals, except for the first two points (5 and 37 minutes).

Self-assembly of the nanodiscs during ligand exchange at the DMSO/air interface. To gain insight into the ligand exchange process of the self-assembled $Cu_{1.1}S$ NDs (already in a 2D hexagonal superlattice) at the DMSO/air interface, we inject a CoTAPc ligand solution into the bulk DMSO and investigate the structural change as a function of reaction time by *in situ* GISAXS measurements. We recorded a series of GISAXS patterns at regular time intervals of 4–6 minutes during ligand exchange, and Fig. 2a–d presents four selected GISAXS patterns, collected at −42, 6, 24 and 276 minutes, respectively. It should be noted that in the present case the reference time ($t = 0$) is the time of ligand injection into the bulk liquid subphase. During ligand

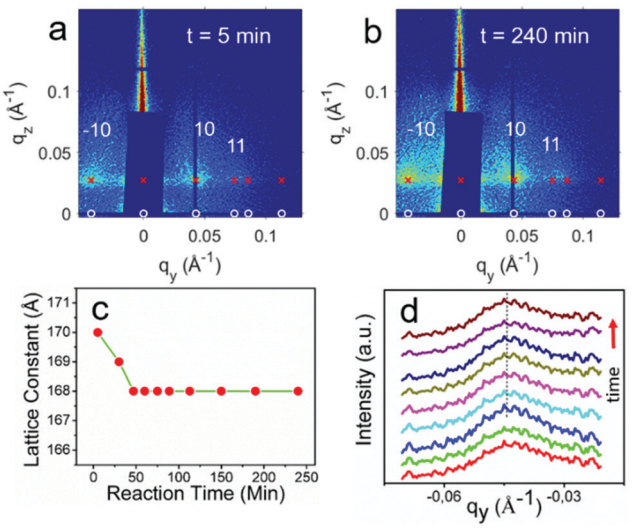

Fig. 1 GISAXS patterns of the NDs during self-assembly for waiting periods of (a) 5 min and (b) 240 min. The white circles (transmitted) and red crosses (reflected) are the simulated diffraction patterns considering a 2D hexagonal superlattice. (c) Temporal evolution of the lattice constants. (d) In-plane line profiles along $-q_y$ through the {10} peak of the GISAXS patterns.

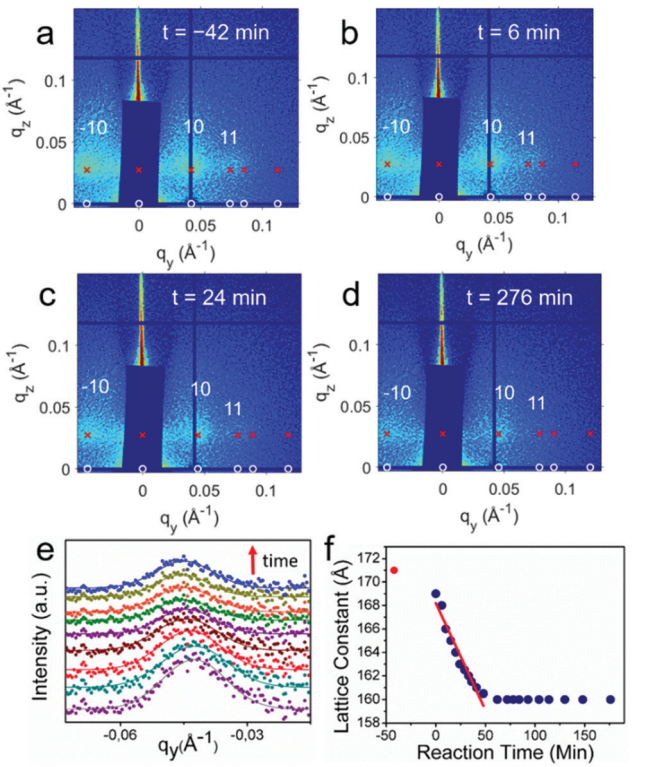

Fig. 2 GISAXS patterns of the ND assemblies during ligand exchange for waiting periods of (a) −42 min, (b) 6 min, (c) 24 min and (d) 276 min. The red crosses (reflected) and white circles (transmitted) are the simulated diffraction patterns considering a 2D hexagonal superlattice. (e) In-plane line profiles along $-q_y$ through the {10} peak of the GISAXS patterns. Peak intensities have been scaled up for clarity. (f) Temporal evolution of the lattice constants with elapsed time.

exchange, the scattering patterns of all the GISAXS images including the images in the intermediate time periods (Fig. S3, ESI†) reveal a high resemblance to the patterns collected during self-assembly (Fig. 1 and 2a). This clearly indicates that the CoTAPc ligands do not significantly change the symmetry of the superlattice during ligand exchange at the liquid/air interface. To determine the transformation of the lattice parameter as a function of reaction time, we again extract the in-plane lattice parameters by simulating and fitting the scattering patterns of each image taking into account DWBA. Additionally, we determine the lattice parameter at different time periods, from the peak position of the corresponding GISAXS line profiles (Fig. 2e) passing through the first correlation peak (−10) along the q_y-direction.

The patterns correspond to a 2D hexagonal superlattice with *P6mm* SG symmetry and oriented with the $[001]_{SL}$-axis perpendicular to the liquid surface with varied lattice parameters (Table S1, ESI†). The temporal evolution of the in-plane superlattice parameters (δ) after ligand injection is presented in Fig. 2f. It illustrates that the lattice parameter shrinks almost linearly from 16.75 ± 0.1 to 16 ± 0.1 nm during the time period of 60 min (see Fig. 2f) at a rate of 0.18 Å min^{-1}. For the remaining waiting period (276 minutes), we have not observed any further major contraction of the superlattice. It is important to note that the hexagonal symmetry of the ND superlattices was conserved during the superlattice contraction *via* ligand exchange with CoTAPc.

Ex situ measurements of the ligand exchanged films. The Raman vibrational spectra of the native and ligand exchanged superlattices are shown in Fig. 3a. The NDs capped with the oleylamine ligand show a sharp peak at 471 cm^{-1}, which can be attributed to the S–S stretching vibration in crystalline CuS nanoparticles (NPs).[32] Several new peaks appearing at 747, 1105, 1336, 1447, 1533 and 1607 cm^{-1} are due to the presence of CoTAPc in the sample through ligand exchange (red curve in Fig. 3a).[33] These Raman spectra of both are in good agreement with those of the existing literature on crystalline copper sulfide and CoTAPc.[25,32,33] Fig. 3b shows the obtained current–voltage (*I–V*) characteristics on a semi-log scale for the corresponding samples. We observe an ohmic behavior of the current with increasing bias voltage. The conductivity of the cross-linked superlattice is higher by about 6 orders of magnitude with respect to the native Olm capped film.

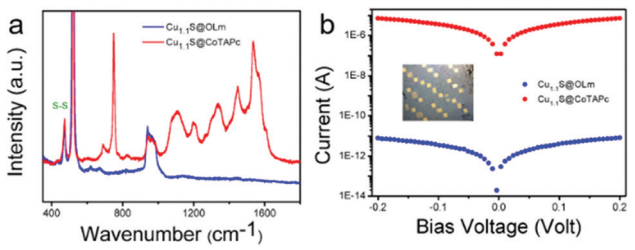

Fig. 3 (a) Raman spectra of $Cu_{1.1}S$ nanodisc thin films before (blue) and after ligand exchange (red). (b) Current–voltage (*I–V*) characteristics of $Cu_{1.1}S$ ND films. Blue circles: Olm-capped $Cu_{1.1}S$ ND films, and red circles: $Cu_{1.1}S$ ND films after ligand exchange. The graph is plotted on a logarithmic scale for better comparison. Inset: Photograph of a substrate with Au contacts for *I–V* measurements.

We determined the structure of the colloidal nanocrystal solution undergoing self-assembly *via* slow solvent evaporation and the superlattice experiencing ligand exchange by CoTAPc ligands as a function of reaction time (276 minutes) and compared our results with few earlier works on the self-assembly of anisotropic nanoparticles. Recently, Maiti *et al.* observed the *in situ* formation of disc shaped single crystalline CuS nano-objects and their self-assembly at liquid–liquid interfaces.[11] Korgel's group reported the self-assembly of disc shaped CuS nanoparticles by using time resolved SAXS and GISAXS, showing the formation of isotropic-to-columnar arrays during solvent evaporation.[34] Li *et al.* also observed the columnar self-assembly of Cu_2S hexagonal nanoplates in which Sn–X complexes act as the native inorganic surface ligands.[35] In contrast to the previous works on disc shaped nanocrystals, we have not found any strong scattering peaks along the out-of-plane (q_z) direction, which undoubtedly rules out the possibility of the formation of columnar assembly by the $Cu_{1.1}S$ NDs. We have not seen similar events even after adding external crosslinking molecules. In our study, we find a very small (∼0.2 nm) contraction of the nanocrystal superlattice parameter during self-assembly *via* solvent evaporation, which is contrary to the solvent evaporation induced assembly of a concentrated solution of spherical PbS NPs (diameter 6.8 nm) at the acetonitrile/air interface.[4] The self-assembly of NCs is attributed to the capillary forces present at the liquid surfaces.[4] On the other hand, this small contraction is consistent with the recent results on cubic PbS NCs (edge length 11.8 nm).[12] It has been proposed that the effective capillary forces are not sufficient enough to displace the relatively large size particles.[4,36,37] We believe that in the present case the small contraction during solvent evaporation is also due to the ineffective capillary forces acting on large diameter (12.7 nm) disc-shaped particles at the air/liquid interface.

In our previous *ex situ* study (prepared in an inert atmosphere/glove box), we observed that similar NDs organise into hexagonal superlattices for self-assembled (without ligand exchange) and ligand exchanged films with copper 4,4′,4″,4‴-tetraaminophthalocyanine (CuTAPc) with similar lattice parameters.[25] In contrast, here we monitored the *in situ* self-assembly and ligand exchange of similar nanodiscs with CoTAPc as adligands directly at the air/liquid interface using synchrotron X-ray scattering to know the formation kinetics of the structural organization. To understand the effect of structural change on the optoelectronic properties, it is noteworthy to correlate the structural, optical and transport behaviors of the $Cu_{1.1}S$ ND superlattices, formed before and after ligand exchange. While Raman spectra (Fig. 3a), particularly the new vibrational peaks above 1000 cm^{-1}, show that the strongly-insulating Olm ligands are replaced by CoTAPc,[25] this removal enhances the current by six orders of magnitude (see Fig. 3b). The significant enhancement in conductivity depicts the efficient charge transport in the coupled superstructures by decreasing the inter-particle separation and increasing electronic coupling among the NDs *via* semiconducting ligands.

In summary, we have monitored the real time structural evolution of $Cu_{1.1}S$ nanodisc superlattices at the DMSO/air interface during self-assembly followed by ligand exchange with CoTAPc molecules. The nanodiscs self-assemble into 2D hexagonal superlattices and their lattice parameters do not change significantly during self-assembly. In contrast, the in-plane lattice parameter of the superlattice contracts isotropically during ligand exchange by preserving the initial structural symmetry with a resultant shrinkage of about 5%. We attribute this contraction to the continuous replacement of oleylamine surface ligands by small CoTAPc molecules. Finally, we demonstrate that the OSC molecules act as electronic coupling agents between the nanodiscs to promote high charge carrier transport across the ordered superlattices.

This work was supported by the DFG under grant SCHE1905/3, SCHE1905/4 and SCHR700/25. We thank the DESY, Hamburg, Germany, for enabling X-ray scattering experiments at P08, Petra-III. We acknowledge the fruitful discussion with F. Bertram, R. Giri and B. Reisz. BMM thanks BMBF for grants 05KS7FK3/05KS10FK2 (LISA spectrometer) and 05K16FK1 (Lambda detector). We thank Mrs Nadler for STEM measurements.

Conflicts of interest

There are no conflicts to declare.

Notes and references

1 M. A. Boles, M. Engel and D. V. Talapin, *Chem. Rev.*, 2016, **116**, 11220–11289.
2 J. Brunner, I. A. Baburin, S. Sturm, K. Kvashnina, A. Rossberg, T. Pietsch, S. Andreev, E. Sturm and H. Colfen, *Adv. Mater. Interfaces*, 2017, **4**, 1600431.
3 J. J. Geuchies, C. van Overbeek, W. H. Evers, B. Goris, A. de Backer, A. P. Gantapara, F. T. Rabouw, J. Hilhorst, J. L. Peters, O. Konovalov, A. V. Petukhov, M. Dijkstra, L. D. A. Siebbeles, S. van Aert, S. Bals and D. Vanmaekelbergh, *Nat. Mater.*, 2016, **15**, 1248–1254.
4 S. Maiti, A. Andre, R. Banerjee, J. Hagenlocher, O. Konovalov, F. Schreiber and M. Scheele, *J. Phys. Chem. Lett.*, 2018, **9**, 739–744.
5 T. Paik, D. K. Ko, T. R. Gordon, V. Doan-Nguyen and C. B. Murray, *ACS Nano*, 2011, **5**, 8322–8330.
6 E. Rabani, D. R. Reichman, P. L. Geissler and L. E. Brus, *Nature*, 2003, **426**, 271–274.
7 D. M. Smilgies, A. T. Heitsch and B. A. Korgel, *J. Phys. Chem. B*, 2012, **116**, 6017–6026.
8 D. Vanmaekelbergh, *Nano Today*, 2011, **6**, 419–437.
9 K. F. Bian, R. P. Li and H. Y. Fan, *Chem. Mater.*, 2018, **30**, 6788–6793.
10 A. G. Kelly, T. Hallam, C. Backes, A. Harvey, A. S. Esmaeily, I. Godwin, J. Coelho, V. Nicolosi, J. Lauth, A. Kulkarni, S. Kinge, L. D. A. Siebbeles, G. S. Duesberg and J. N. Coleman, *Science*, 2017, **356**, 69–72.
11 S. Maiti, M. K. Sanyal, N. Varghese, B. Satpati, D. Dasgupta, J. Daillant, D. Carriere, O. Konovolov and C. N. R. Rao, *J. Phys.: Condens. Matter*, 2013, **25**, 395401.
12 S. Maiti, S. Maiti, A. Maier, J. Hagenlocher, A. Chumakov, F. Schreiber and M. Scheele, *J. Phys. Chem. C*, 2018, **123**, 1519–1526.
13 M. C. Weidman, Q. Nguyen, D. M. Smilgies and W. A. Tisdale, *Chem. Mater.*, 2018, **30**, 807–816.
14 W. N. Wenger, F. S. Bates and E. S. Aydile, *Langmuir*, 2017, **33**, 8239–8245.
15 M. Scheele, W. Brutting and F. Schreiber, *Phys. Chem. Chem. Phys.*, 2015, **17**, 97–111.
16 K. Whitham, D. M. Smilgies and T. Hanrath, *Chem. Mater.*, 2018, **30**, 54–63.
17 Y. X. Zhao and C. Burda, *Energy Environ. Sci.*, 2012, **5**, 5564–5576.
18 W. van der Stam, S. Gudjonsdottir, W. H. Evers and A. J. Houtepen, *J. Am. Chem. Soc.*, 2017, **139**, 13208–13217.
19 Y. Bekenstein, O. Elimelech, K. Vinokurov, O. Millo and U. Banin, *Z. Phys. Chem.*, 2015, **229**, 179–190.
20 Y. Xie, A. Riedinger, M. Prato, A. Casu, A. Genovese, P. Guardia, S. Sottini, C. Sangregorio, K. Miszta, S. Ghosh, T. Pellegrino and L. Manna, *J. Am. Chem. Soc.*, 2013, **135**, 17630–17637.
21 O. O. Otelaja, D. H. Ha, T. Ly, H. Zhang and R. D. Robinson, *ACS Appl. Mater. Interfaces*, 2014, **6**, 18911–18920.
22 M. R. Jones, R. J. Macfarlane, A. E. Prigodich, P. C. Patel and C. A. Mirkin, *J. Am. Chem. Soc.*, 2011, **133**, 18865–18869.
23 S. Kan, T. Mokari, E. Rothenberg and U. Banin, *Nat. Mater.*, 2003, **2**, 155–158.
24 M. B. Sigman, A. Ghezelbash, T. Hanrath, A. E. Saunders, F. Lee and B. A. Korgel, *J. Am. Chem. Soc.*, 2003, **125**, 16050–16057.
25 S. Maiti, S. Maiti, Y. Joseph, A. Wolf, W. Brütting, D. Dorfs, F. Schreiber and M. Scheele, *J. Phys. Chem. C*, 2018, **122**, 23720–23727.
26 A. Andre, C. Theurer, J. Lauth, S. Maiti, M. Hodas, M. S. Khoshkhoo, S. Kinge, A. J. Meixner, F. Schreiber, L. D. A. Siebbeles, K. Braun and M. Scheele, *Chem. Commun.*, 2017, **53**, 1700–1703.
27 Z. Jiang, *J. Appl. Crystallogr.*, 2015, **48**, 917–926.
28 S. Maiti, M. K. Sanyal, M. K. Jana, B. Runge, B. M. Murphy, K. Biswas and C. N. R. Rao, *J. Phys.: Condens. Matter*, 2017, **29**, 095101.
29 G. Renaud, R. Lazzari and F. Leroy, *Surf. Sci. Rep.*, 2009, **64**, 255–380.
30 M. P. Tate, V. N. Urade, J. D. Kowalski, T. C. Wei, B. D. Hamilton, B. W. Eggiman and H. W. Hillhouse, *J. Phys. Chem. B*, 2006, **110**, 9882–9892.
31 S. K. Sinha, E. B. Sirota, S. Garoff and H. B. Stanley, *Phys. Rev. B: Condens. Matter Mater. Phys.*, 1988, **38**, 2297–2311.
32 P. Kumar and R. Nagarajan, *Inorg. Chem.*, 2011, **50**, 9204–9206.
33 M. Imadadulla, M. Nemakal and L. K. Sannegowda, *New J. Chem.*, 2018, **42**, 11364–11372.
34 A. E. Saunders, A. Ghezelbash, D. M. Smilgies, M. B. Sigman and B. A. Korgel, *Nano Lett.*, 2006, **6**, 2959–2963.
35 X. M. Li, H. B. Shen, J. Z. Niu, Y. G. Zhang, H. Z. Wang and L. S. Li, *J. Am. Chem. Soc.*, 2010, **132**, 12778–12779.
36 M. K. Sanyal, S. K. Sinha, K. G. Huang and B. M. Ocko, *Phys. Rev. Lett.*, 1991, **66**, 628–631.
37 F. Bresme and M. Oettel, *J. Phys.: Condens. Matter*, 2007, **19**, 413101.

